Non-covalently functionalized graphene strengthened poly(vinyl alcohol)

Xiaodong Wang [a], Xianhu Liu [a,*], Hongyue Yuan [a], Hu Liu [a], Chuntai Liu [a,*], Tingxi Li [b], Chao Yan [c], Xingru Yan [d], Changyu Shen [a], Zhanhu Guo [d,*]

[a] National Engineering Research Center for Advanced Polymer Processing Technology, Zhengzhou University, Zhengzhou 450002, China
[b] College of Materials Science and Engineering, Shandong University of Science and Technology, Qingdao 266590, China
[c] School of Material Science and Engineering, Jiangsu University of Science and Technology, Zhenjiang, Jiangsu, China
[d] Integrated Composites Laboratory (ICL), Department of Chemical & Biomolecular Engineering, University of Tennessee, Knoxville, TN 37996, USA

HIGHLIGHTS

- Non-covalently functionalized rGO PVA nanocomposites were prepared by solution mixing.
- Uniform dispersion of rGO was achieved with the assistance of poly(sodium 4-styrenesulfonate).
- Strong rGO-PVA interactions and effective load transfer from rGO to PVA significantly improved the mechanical properties.

GRAPHICAL ABSTRACT
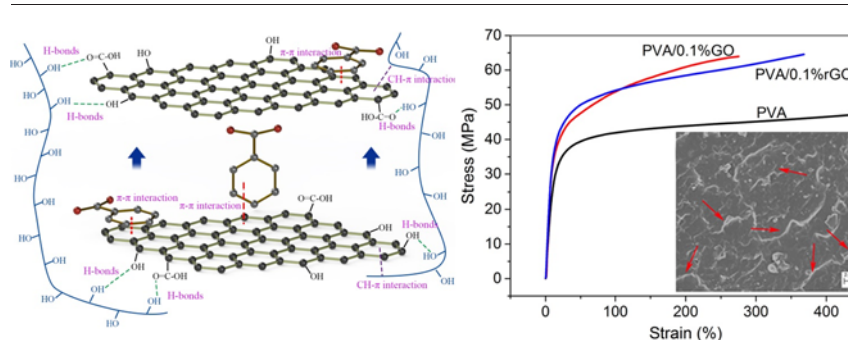
ARTICLE INFO

ABSTRACT

In this work, non-covalently functionalized reduced graphene oxide (rGO) reinforced poly(vinyl alcohol) (PVA) nanocomposites were prepared by solution mixing. The agglomeration of graphene sheets was prevented by using surface modifying agent poly(sodium 4-styrenesulfonate) (PSS). The improved mechanical properties, including the Young's modulus and tensile strength of the PVA/rGO nanocomposites compared to neat PVA were attributed to the strong interactions between PVA and rGO such as π–π, hydrogen bonding, and CH–π. A 55% maximum increase in the modulus was obtained by adding only 0.1 wt% rGO, and an increase of 48% in tensile strength was achieved by adding 0.3 wt% rGO. In addition, the thermal properties of the nanocomposites were also improved, which was attributed to the restriction of graphene oxide (GO)/rGO sheets on the chain mobility of polymers on the GO/rGO sheets surface.

© 2017 Elsevier Ltd. All rights reserved.

1. Introduction

Graphene has attracted a lot of attention since the direct observation and characterization of a mechanically exfoliated graphene monolayer by Novoselov et al. in 2004 [1]. This two-dimensional (2D) sheet composed of sp^2-hybridized carbon atoms and arrayed in a honeycomb pattern is the world's thinnest, strongest, and stiffest material. Because of its superior properties of electronic, mechanical, optical and transparent nature, graphene has already revealed a great number of potential applications with possible uses in touch screen [2–4], capacitors [5,6], fuel cells [7–9], batteries [10–12], advanced adsorbents [13a,b], sensors [13c,14a], functional metacomposites [14b,c], and flexible electronics [15,16]. Several methods have been reported for preparing graphene sheets. Although micromechanical cleavage can produce high-quality and defect-free graphene, it cannot be used for large quantity of graphene from graphite. In order to obtain effectively large quantities

* Corresponding authors.
E-mail addresses: xianhu.liu@zzu.edu.cn (X. Liu), ctliu@zzu.edu.cn (C. Liu),
zguo10@utk.edu (Z. Guo).
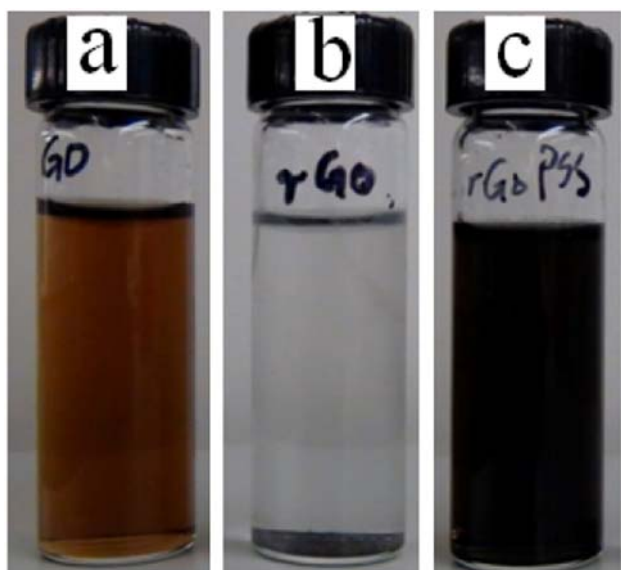
Fig. 1. Photographs of water dispersions of (a) GO, (b) rGO, and (c) rGO with PSS. (For interpretation of the references to color in this figure, the reader is referred to the web version of this article.)

of graphene, an approach for the preparation of nanoplatelets from graphite by a chemical method is more scalable and popular.

Recently, to use graphene as a nano-filler in polymer matrix has become a rapidly expanding field [17–21]. The properties of graphene nanocomposites will depend on the dispersion ability of graphene in the polymer matrix. For example, Liang et al., for the first time, reported the simple and effective processing method for the fabrication of poly(-vinyl alcohol) (PVA)/graphene oxide (GO) nanocomposites and revealed a significant enhancement of mechanical properties of PVA/GO nanocomposites at fairly low concentrations of GO [22]. GO still possesses similar layered structure of graphene, while the basal planes of GO sheets are heavily decorated with oxygen-containing groups, which cause these oxidized layers to become hydrophilic and enable the uniform dispersion of graphene sheets in water with moderately ultrasonicating. Meanwhile, the extended aromatic system of the graphene is disrupted due to the transformation of carbon atoms from sp2 to sp3 hybridization during the oxidation, which dramatically alters the structure of the carbon plane and then affects the properties of its nanocomposites.

The original aromatic graphene network could be partially restored by chemical deoxygenation. It is possible to access the intrinsic structure via graphite oxide exfoliation and a subsequent solution-based chemical reduction [23–27]. It is expected that the properties of PVA/reduced GO (rGO) nanocomposites become superior after the recovery of a conjugated structure. However, the reduction reaction along with the removal of O-containing functional groups on GO surface will reduce the hydrophilicity of sheets, which eventually leads to their irreversible agglomeration or even restacking to graphite via strong π–π stacking and van der Waals interactions. Thus, some methods have been used for the prevention from aggregation by functionalizing graphene sheet surfaces through covalent [28,29] or noncovalent approaches [21,23, 30]. Although covalent and noncovalent approaches would ensure the good dispersion of the graphene sheets in aqueous media, the noncovalent functionalization is a better choice to keep the intrinsic structure of graphene and easier to carry out. Some chemical agents like sulfonated polyaniline [21], poly(sodium 4-styrenesulfonate) (PSS) [23], tryptophan [30], 1-(2-pyridylazo)-2-naphthol (PAN) [31], or aromatic polymers have been used for noncovalent surface modification of graphene. Among them, the affinities of PSS toward the basal planes of graphene, as well as toward solvent or matrix are excellent. In addition, graphene based composites combined with PSS could be used for electronic components [32] or medical applications [33]. Therefore, in this study, we report the fabrication of the polymer composite system featuring PVA as matrix, GO/rGO as fillers and PSS as noncovalent agent. The properties of the PVA/GO nanocomposite and PVA/rGO nanocomposite were studied and the molecular interactions in nanocomposite were discussed.

2. Experimental section

2.1. Materials

Graphite, PSS ($M_w = 1{,}000{,}000$), and PVA ($M_w = 89{,}000$–$98{,}000$, $99+\%$ hydrolyzed) were purchased from Sigma Aldrich. Chemical agents used in this study included concentrated sulfuric acid (H_2SO_4), potassium permanganate ($KMnO_4$), hydrochloric acid (HCl), 30% hydrogen peroxide (H_2O_2), and hydrazine hydrate (85%), which were also purchased from Sigma Aldrich. The materials were used directly without any further purification.

2.2. Reduction of exfoliated graphite oxide

In the oxidation process, GO was prepared from flake graphite using the modified Hummers method [34–38]. In the reduction process, 100 mg GO and 200 mL deionized (DI) water were added into a 250 mL round-bottom flask to form an inhomogeneous dispersion. The solution with the inhomogeneously dispersed GO was placed in an ultrasonic bath. After 1 h, the suspension turned yellow and no aggregation at the bottom of the flask was observed, indicating the uniform dispersion of GO. The exfoliated graphite oxide was termed as GO assuming that the nanoplatelets no longer existed as aggregated or stacked forms. Next, 1.0 g PSS (10:1, PSS:GO) was added to the above solution. Vigorous stirring was applied for 1 h until the PSS was fully
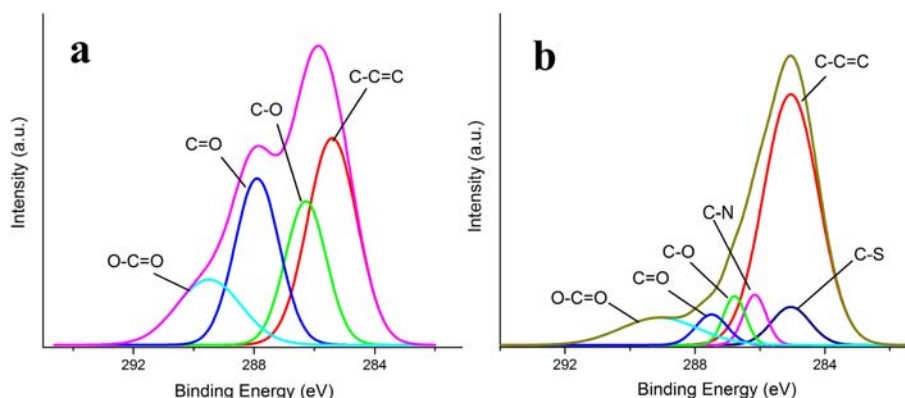
Fig. 2. The C1s XPS spectra of (a) GO and (b) rGO.

Table 1
Assignment of various components of C1s in GO and rGO and the ratio of C to other elements in GO and rGO. The integrated intensity values (%) are displayed.

Sample	Functional groups								
	O=C—O	C=O	C—O	C—C=C	C—S	C—N	C/O	C/S	C/N
GO	289.5	287.6	286.3	284.5	–	–	2.2	–	–
Peak area (%)	15.18	26.62	21.32	36.88	–	–			
rGO	289.1	287.5	286.8	284.5	285.0	286.2	7.7	32.8	41.9
Peak area (%)	10.30	4.69	5.25	67.04	7.13	5.58			

dissolved in the solution. Hydrazine hydrate was blended with the GO/PSS solution, and then heated in an oil bath at 95 °C for 24 h. The black rGO powders were washed with DI water to remove any excess hydrazine monohydrate and excess PSS via filtration through a poly(vinylidene fluoride) (PVDF) membrane (0.4 μm pore size, Fisher Scientific) and dried in a desiccator with a detachable stopcock valve for 24 h. The rGO film was separated by peeling it from the membrane.

2.3. Preparation of PVA/GO and PVA/rGO films

PVA was added in DI water at 80 °C and stirred constantly for 2 h till completely dissolved. A predetermined weight of GO or rGO was dissolved in DI water in an ultrasonic bath for 2 h. The predetermined content of GO or rGO in the composite films was 0.1, 0.3, 0.5 and 1 wt%, respectively. The mixtures were shaken for 10 min, degassed in an ultrasonic bath for 20 min, cast into Petri dishes, and then dried at 50 °C in an oven until no change could be perceived in their weights. Then the PVA/GO and PVA/rGO nanocomposites were produced. Pure PVA films were prepared as a reference following the same procedures as the aforementioned ones for preparing the nanocomposites films.

2.4. Characterization

X-ray photoelectron spectroscopy (XPS) was performed using a Perkin Elmer PHI5400 with a 300 W monochromatic Mg Kα X-ray source. The RBD AugerScan software was used to analyze the data. The Gauss equation was used to fit the peaks of each component profile. Micro Raman spectroscopy was carried out using a Thermo Scientific DXR Raman microscope with a DXR 532 nm laser mounted on it. Fourier transform infrared (FT-IR) spectra of the nanocomposites in ATR mode were obtained using a Bruker Tensor 27 FT-IR. A dynamic mechanical analyzer (DMA Q800, TA Instruments) was used to characterize the stress-strain behavior of the samples. The samples were cut into rectangular strips 30 mm × 3 mm in dimension for a film tension test using DMA in the strain rate mode. Five samples were tested for each group, and the tensile modulus and tensile strength were recorded.

During the tension test, the samples were preloaded at 0.0001 N, the force ramp rate was 0.2 N/min, and the temperature was 30 °C. Thermogravimetric analysis tests were carried out in TGA Q50 (TA, USA). Samples were weighed at 9.5–10.0 mg and placed in platinum pans. The tests were equilibrated at 50 °C and heated to 800 °C at a heating rate of 10 °C/min under N_2 atmosphere (20 mL/min).

3. Results and discussion

3.1. Dispersion of rGO with PSS

Fig. 1 shows the comparative stability of the GO suspension. Suspension difference is visible. The GO aqueous suspension is very stable and shows a brown color (Fig. 1(a)). The rGO without any stabilizer almost completely precipitated (Fig. 1b) due to the rapid and irreversible aggregation of the rGO sheets. However, as shown in Fig. 1c, the rGO
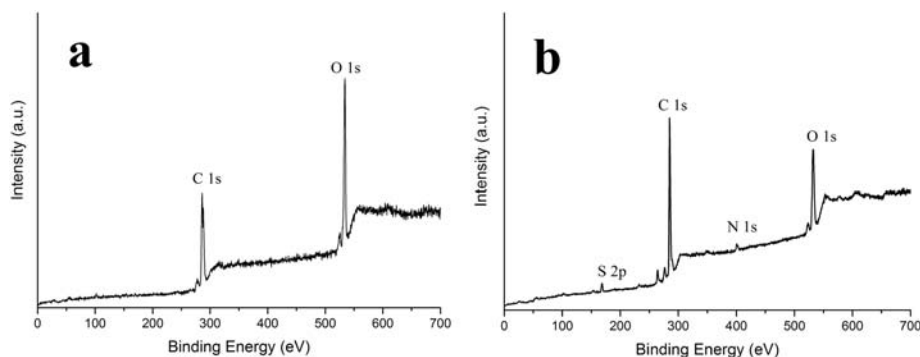
Fig. 3. The XPS survey scan of (a) GO, and (b) rGO.
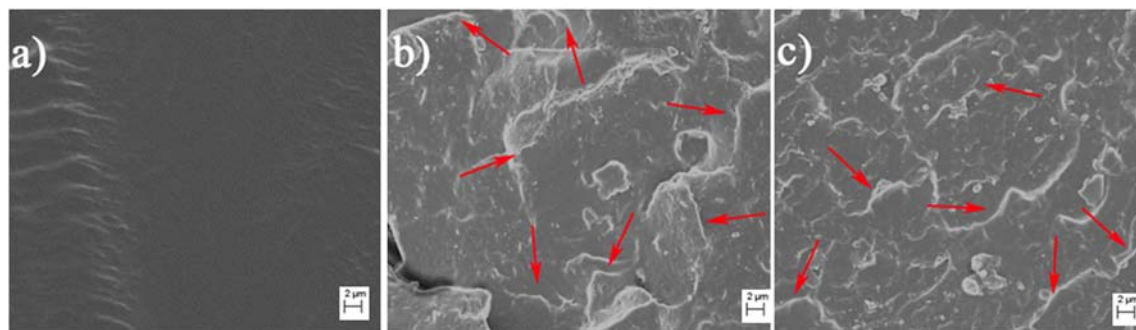
Fig. 4. SEM images of the fracture surfaces of (a) neat PVA, (b) PVA/0.5% GO, and (c) PVA/0.5% rGO films. (For interpretation of the references to color in this figure, the reader is referred to the web version of this article.)

with PSS suspension remained stable and black, almost without precipitation after storing for one week.

3.2. Structure and morphology

XPS can be used to identify the chemical elements and to assess their contents [39,40]. The C1s XPS spectra for GO and rGO are used to analyze the degree of carbon oxidation. Three different functional groups, i.e., C—O, C=O, and COOH are observed (Fig. 2), and their peak positions are listed in Table 1. The intrinsic carbon peak corresponds to the non oxygenated ring C (C=C—C at 284.5 eV). The peaks of the oxygen functionalities of GO are similar to those of the oxygen functionalities of rGO, and correspond to the C—O bonds (C—O at ~286 eV), carbonyl C (C=O at ~287 eV), and carboxylate carbon (O=C—O at ~289 eV) [23,39,40].

Besides the intrinsic carbon peak, the C1s XPS spectrum of the GO sample exhibits two other dominant peaks due to a high level of oxygen (Fig. 2a). A broad shoulder in the range from 286 to 292 eV contains several components with the corresponding peak positions and areas listed in Table 1. The content ratio of C to O in the GO samples was obtained by calculating the area ratio of C to O. In contrast, the shoulder peak in the rGO sample, which was associated with the oxygen functionalities C—O, C=O, and COOH groups, decreased significantly. The peak associated with C=C—C became predominant. The content ratio of C to O increased from 2.2 in GO to 7.7 in rGO (Table 1), which indicated that most of the oxygen functionalities in the GO had been removed. In addition, a very low content of sulfur and nitrogen was found in the rGO due to the PSS coating on the carbon sheets and the residual hydrazones (Fig. 2b) [40]. The content ratios of C to S and C to N in rGO were 32.8 and 41.9 (Table 1), respectively. Since S and N might have been introduced during the reduction process, XPS was also carried out. The existing two elements can be assigned to the C—S (285.5 eV) and C—N (286.2 eV) species whose peak positions, peak area and elements ratio are listed in Table 1. Fig. 3 shows the survey XPS spectra of the GO and rGO samples containing four elements: C 1s, O 1s, S 2p, and N 1s. For GO, the intensity of the O peak is higher than that of the C peak, indicating that GO is highly oxidized. As a comparison, the ratio of C to O intensity on rGO sheets became higher and new peaks appeared at ~180 eV (S 2p) and ~400 eV (N 1s), which evidenced a reduction reaction [28, 41]. And only very small amount of PSS was retained on the rGO sheet surface corresponding to the disappearance of S peak after rGO sheets were rinsed repeatedly.

Fig. 4 shows the SEM images of the fractured surfaces of neat PVA, PVA/GO film with 0.5% GO, and PVA/rGO film with 0.5% rGO, respectively. The surface morphologies of the fractured surfaces of the samples were significantly affected by the nanofiller sheets. It can be seen from Fig. 4b and c that the individual GO and rGO sheets were fully exfoliated and well dispersed in the PVA matrix (as indicated by red arrows). The GO sheets were coated with PVA, indicating the existing interfacial interactions between GO sheets and PVA chains [42–44]. The fractured surface of PVA/rGO was smoother than that of the PVA/GO composites due to the good miscibility between PVA and PSS. Compared with the fracture surface of GO, the rGO sheets indicated by red arrows were not very clear, which was attributed to the more CH–π interaction between the rGO sheets and PVA and easier encapsulation in the PVA matrix. No agglomeration was found on the rGO fracture surface.

Fig. 5a shows the Raman spectra of pristine graphite, GO, and rGO. The spectra of graphite display the typical features: a prominent G peak at 1583 cm^{-1}, which is due to the sp^2 C—C bonds, and a weak peak at 1351 cm^{-1} for the D band. The G peak is due to the doubly degenerated zone center E2g vibration mode and the D peak is due to structural defects in the graphite [45]. The D and G bands were also observed at GO and rGO. After the chemical oxidation and reduction, the G band was broadened and the D band became prominent and wide. The positions of the D, G, and 2D bands were at 1351, 1587, and 2692 cm^{-1} for GO, respectively, and at 1343, 1571, and 2676 cm^{-1} for rGO,
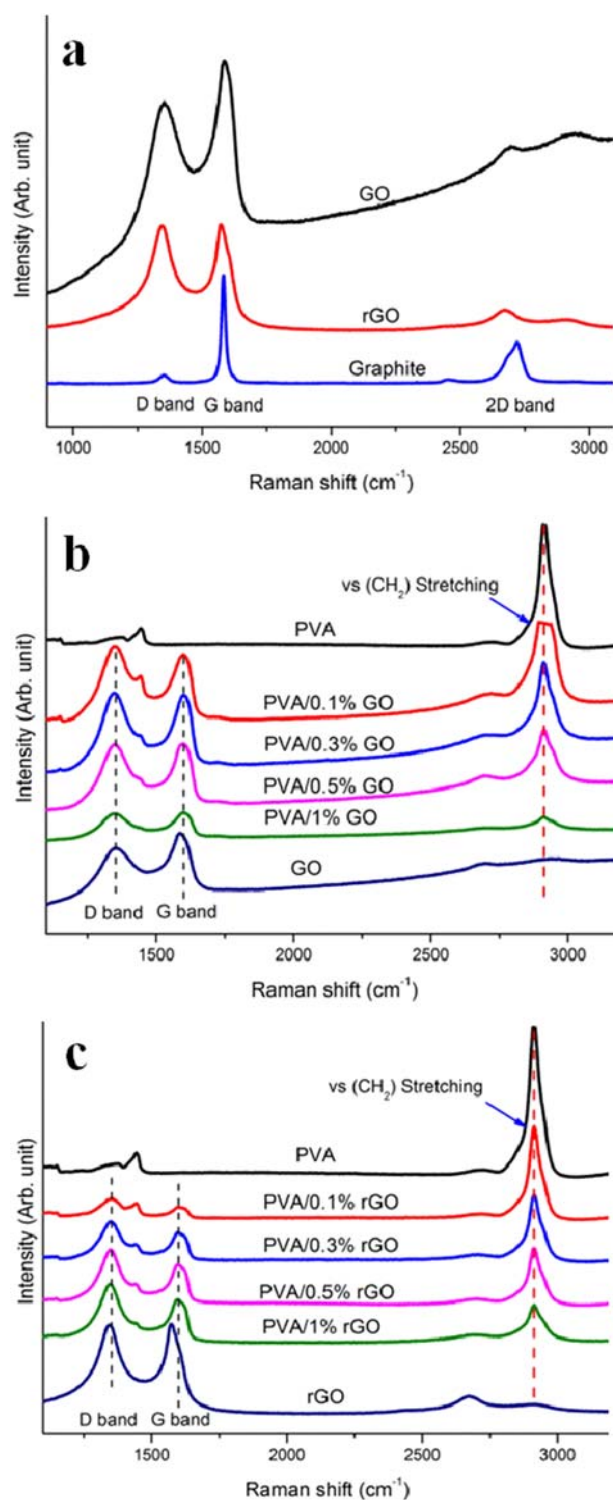
Fig. 5. Raman spectra of (a) graphite, GO, and rGO; (b) PVA/GO composites; and (c) PVA/rGO composites.

respectively. The ratio of D- to G-band intensity (ID/IG), which indicates the size of the in-plane sp^2 domains, increased from 0.12 for graphite to 0.88 for GO and 1.02 for rGO due to the increasing number of defects or the increasing number of small-sized aromatic domains during the oxidation and reduction processes.

Raman spectroscopy was also carried out to investigate the interaction between the matrix and graphene sheets. Compared to neat GO or the rGO, the G band of the sheets in both composites shifted by about 14 cm^{-1} for the PVA/GO composites, and 9 cm^{-1} for the PVA/rGO
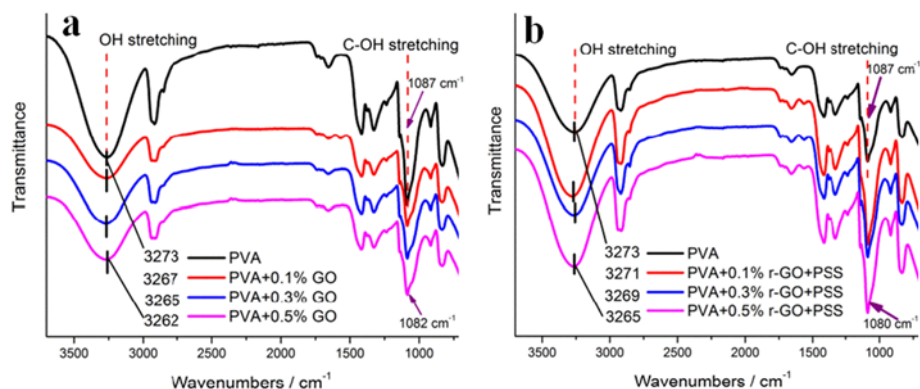
Fig. 6. FT-IR spectra of PVA and their composites: (a) PVA/GO and (b) PVA/rGO composites.

composites, whereas the D band only shifted slightly (Fig. 5b and c). The GO or rGO sheets were covered by the chains of polymer matrix, which affected the vibration movement of the C—C bonds in the carbon plane due to the hydrogen bonding between the —OH or —COOH groups of graphene and the —OH groups of the polymer matrix. The hydrogen bonding in the PVA/GO composites was more than that in the PVA/rGO composites because part of the O-containing functional groups on rGO sheet surface was removed. For this reason, the peak shift of the PVA/GO composites was more obvious than that of PVA/rGO. There was a nearly identical structure in graphene—the benzene ring in PSS. This similar structure induces a strong π–π stacking interaction, also known as an aromatic interaction, which is stronger than other noncovalent interactions [46]. At the same time, a characteristic peak at 2910 cm^{-1} in both composites was attributed to the intrinsic νs (CH) stretch band of the PVA [47]. The peak intensities in both composites were suppressed gradually with the addition of GO or rGO due to the CH–π interactions.

Fig. 6 shows the FT-IR spectra. The characteristic peak of the hydroxyl band at around 3265 cm^{-1} shifted to a lower wavenumber as the filler loading increased. The band around 1050 to 1100 cm^{-1}, which was attributed to the —C—OH stretching, had a similar shift. In addition to the shifts of these peaks, no new peaks observed indicated that the PSS did not react with the PVA. The shift of the hydroxyl bond and —C—OH stretching bond indicated the existence of hydrogen bonding between hydroxyl bands in the PVA and the remaining oxygen-functional groups in the GO/rGO composites [48,49]. The characteristic peak of the hydroxyl band in the PVA/GO composites shifted to a lower wavenumber compared to the PVA/rGO results due to the more intensity of hydrogen bonding in the PVA/GO composites.

3.3. Thermal properties

Thermogravimetric analysis (TGA) was used to characterize the thermal stability of graphite, GO, rGO, PVA, PVA/GO and PVA/rGO nanocomposites, as shown in Fig. 7. With more oxygenated functionalities, GO has less thermal stability than graphite and rGO. As it can be seen, pure graphite did not show any weight loss until 700 °C. For GO, a slight weight loss observed below 100 °C corresponded to the loss of moisture, and a significant weight loss was noted around 231 °C which was due to the decomposition of O-containing functional groups on the GO surface. As a comparison, a gradual weight loss from 200 to 350 °C for rGO is attributed to the decomposition of residual O-containing function groups on the rGO surface. The total weight loss of GO and rGO was 53% and 36% respectively. Although GO is decomposed at a lower temperature than PVA, the temperature of the maximum degradation rate for the PVA/GO nanocomposites is increased compared to that of neat PVA. This indicates that the addition of GO can improve the thermal stability of PVA, which is attributed to the restricted chain mobility of polymers near the GO sheets surface [50–55]. However, for the PVA/rGO

nanocomposites, the decomposition of PVA/rGO composites is slightly lower than that of neat PVA owing to the restoration of the conjugated structure and thermal conductivity.

3.4. Mechanical properties

Fig. 8 shows that the mechanical properties of the PVA/GO and PVA/rGO composites are improved significantly with the addition of GO and rGO. As shown in Fig. 8a, the modulus of the PVA/GO composites increased with increasing the content of GO, from 1.74 GPa for neat PVA to a maximum value of 2.17 GPa for the PVA/GO nanocomposites with 0.5 wt% GO—an increase of 25%. The tensile strength of the PVA/GO nanocomposites had a similar trend to the modulus, which was increased by 44% from neat PVA to a PVA/GO nanocomposites with 0.5 wt% GO. In contrast, the modulus of PVA/rGO nanocomposites was increased sharply by 55% to 2.69 GPa with the addition of 0.1 wt% rGO, and then decreased slightly with a further increase in rGO content (Fig. 8b). However, the tensile strength increased by 48%, from 65.7 MPa for neat PVA to 97.5 MPa for the composites, with 0.3 wt% rGO, and then decreased to 84.8 GPa at 0.5 wt% rGO. This indicated that rGO sheets could be uniformly dispersed in a polymer matrix in the presence of PSS at low filler contents. Because of the uniform distribution in the matrix of rGO sheets, the strong interfacial interactions between rGO and PVA, and effective load transfer from rGO to PVA led to a significant improvement in the mechanical properties. Due to partial restoration of the intrinsic aromatic structure, rGO showed a prominently improved rigidity effect on the nanocomposites. However, with increasing the content of rGO, the distance between rGO sheets gets smaller and the interaction between rGO sheets becomes stronger which make rGO
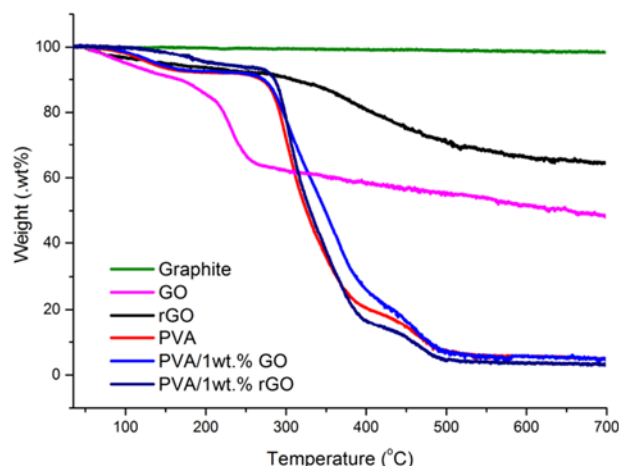
Fig. 7. TGA curves of graphite, GO, rGO, and the PVA nanocomposites.
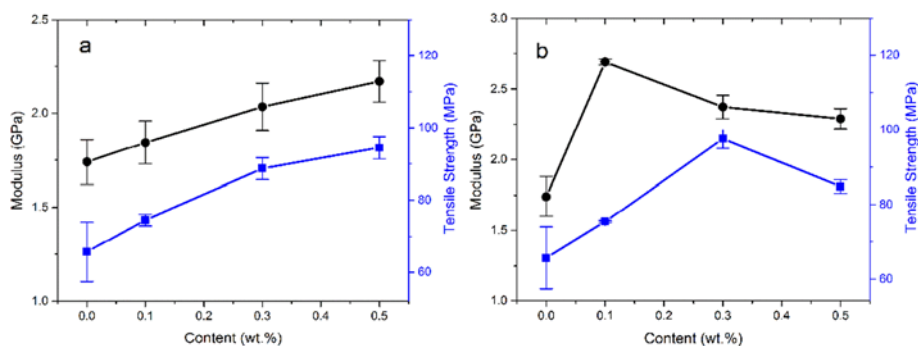
Fig. 8. Young's moduli and tensile strength of (a) PVA/GO and (b) PVA/rGO films.

sheets tend to agglomerate even surrounding rGO sheets with PSS. Thus, the mechanical properties of PVA/rGO nanocomposites with the incorporation of 0.5 wt% rGO appeared to decrease. The mechanical properties of PVA/rGO nanocomposites with addition of low content could be improved significantly.

3.5. Interactions in the composites

The schematic diagram illustrated in Fig. 9 shows the π–π interactions, hydrogen bonding, and CH–π interactions among the materials [56–59]. PSS is amphiphilic molecules. On one hand, the affinity of the hydrophobic aromatic benzene ring of PSS toward the hydrophobic hexatomic rings of the rGO sheets could be maintained with a noncovalent π–π interaction. On the other hand, the hydrophilic —COO— groups of PSS enabled the rGO sheets to remain stably suspended in water and prevented them from restoring the π–π interaction that irreversibly restacked the rGO monolayer sheets to graphite again. The dispersion of rGO sheets was improved by a noncovalent π–π interaction that did not disrupt the sp^2 network of the rGO. When PVA was added in the dispersion, hydrogen bonding was present between the hydroxyl groups in PVA and the remaining oxygen functional groups on the rGO sheets. Furthermore, the bone chains were attracted to the basal planes, the hexatomic rings of rGO, hence the CH–π interaction between the PVA molecular chains and rGO sheets could be attributed to the dispersion of the rGO sheets in the matrix.

4. Conclusions

The PVA nanocomposites filled by GO/rGO sheets were investigated. Based on the noncovalently functionalizing method, rGO sheets can be well-dispersed in the PVA matrix. This method can avoid the agglomeration of rGO during the PVA/GO reduction process. The interactions among the molecules prevented the rGO sheets from restacking, allowing them to be well-dispersed. The SEM images showed good dispersion of rGO sheets in the PVA matrix. The XPS, Raman and FTIR study evidenced a strong interfacial interaction between PSS and rGO. The TGA study showed that GO can be the heat barrier in the PVA matrix due to the high aspect ratio (l/d > 1000) and the restriction on the mobility of polymers chain. The mechanical property was enhanced by 55% in Young's modulus and 15% in tensile strength by the addition of only 0.1 wt% rGO. The strong interfacial interactions between rGO and PVA, and effective load transfer from rGO to PVA led to a significant improvement in mechanical properties.
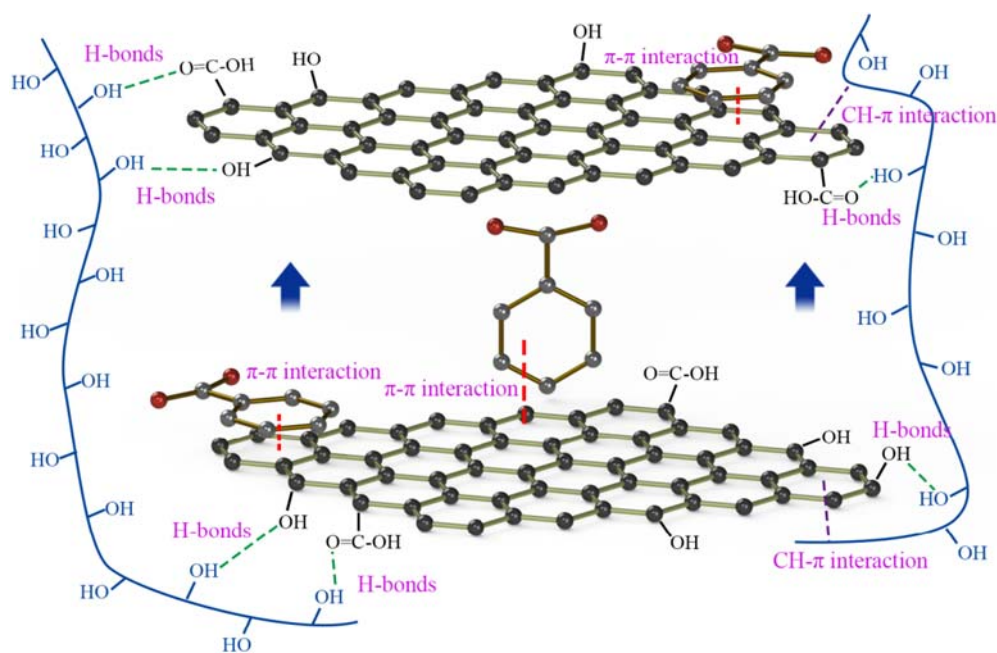
Fig. 9. Schematic diagram of the interactions among the rGO sheets, PSS molecules, and PVA molecules.

References

[1] K.S. Novoselov, A.K. Geim, S.V. Morozov, D. Jiang, Y. Zhang, S.V. Dubonos, I.V. Grigorieva, A.A. Firsov, Electric field effect in atomically thin carbon films, Science 306 (2004) 666–669.

[2] S. Huh, J. Park, K.S. Kim, B.H. Hong, S.B. Kim, Selective n-type doping of graphene by photo-patterned gold nanoparticles, ACS Nano 5 (2011) 3639–3644.

[3] S. Bae, H. Kim, Y. Lee, Xu XF, J.S. Park, Y. Zheng, J. Balakrishnan, T. Lei, H.R. Kim, Y.I. Song, Y.J. Kim, K.S. Kim, B. Ozyilmaz, J.H. Ahn, B.H. Hong, S. Iijima, Roll-to-roll production of 30-inch graphene films for transparent electrodes, Nat. Nanotechnol. 5 (2010) 574–578.

[4] C.F. Zhang, T.M. Higgins, S.H. Park, S.E. O'Brien, D.H. Long, J. Coleman, V. Nicolosi, Highly flexible and transparent solid-state supercapacitors based on RuO₂/PEDOT: PSS conductive ultrathin films, Nano Energy 28 (2016) 495–505.

[5] X.Y. Zhang, P. Samori, Graphene/polymer nanocomposites for supercapacitors, Chem. Aust. 3 (2017) 362–372.

[6] H. Banda, D. Aradilla, A. Benayad, Y. Chenavier, B. Daffos, L. Dubois, F. Duclairoir, One-step synthesis of highly reduced graphene hydrogels for high power supercapacitor applications, J. Power Sources 360 (2017) 538–547.

[7] Qu LT, Y. Liu, J.B. Baek, L.M. Dai, Nitrogen-doped graphene as efficient metal-free electrocatalyst for oxygen reduction in fuel cells, ACS Nano 4 (2010) 1321–1326.

[8] R.L. Liu, D.Q. Wu, X.L. Feng, K. Mullen, Nitrogen-doped ordered mesoporous graphitic arrays with high electrocatalytic activity for oxygen reduction, Angew. Chem. Int. Ed. 49 (2010) 2565–2569.

[9] T. Liu, K. Yu, L. Gao, H. Chen, N. Wang, L.H. Hao, T.X. Li, H.C. He, Z.H. Guo, A graphene quantum dot decorated SrRuO₃ mesoporous film as an efficient counter electrode for high-performance dye-sensitized solar cells, J. Mater. Chem. A 5 (2017) 17848–17855.

[10] E. Yoo, J. Kim, E. Hosono, H.-S. Zhou, T. Kudo, I. Honma, Large reversible Li storage of graphene nanosheet families for use in rechargeable lithium ion batteries, Nano Lett. 8 (2008) 2277–2282.

[11] S.J. Woltornist, A.J. Oyer, J.-M.Y. Carillo, A.V. Dobrynin, D.H. Adamson, Conductive thin films of pristine graphene by solvent interface trapping, ACS Nano 7 (2013) 7062–7066.

[12] M. Li, X. Xiao, Y. Liu, W. Zhang, Y. Zhang, L. Chen, Ternary perovskite cobalt titanate/graphene composite material as long-term cyclic anode for lithium-ion battery, J. Alloys Compd. 700 (2017) 54–60.

[13] (a) G. Yu, Y. Lu, J. Guo, M. Patel, A. Bafana, X. Wang, B. Qiu, C. Jeffryes, S. Wei, Z. Guo, E.K. Wujcik, Adv. Compos. Hybrid Mater. (2017) https://doi.org/10.1007/s42114-017-0004-3 in press;
(b) J. Huang, Y. Cao, Q. Shao, X. Peng, Z. Guo, Magnetic nanocarbon adsorbents with enhanced hexavalent chromium removal: morphology dependence of fibrillar vs particulate structures, Ind. Eng. Chem. Res. 56 (2017) 10689–10701 and;
(c) X. Su, J. Ren, X. Meng, X. Ren, F. Tang, A novel platform for enhanced biosensing based on the synergy effects of electrospun polymer nanofibers and graphene oxides, Analyst 138 (2013) 1459–1466.

[14] (a) M. Zhou, Y.M. Zhai, S.J. Dong, Electrochemical sensing and biosensing platform based on chemically reduced graphene oxide, Anal. Chem. 81 (2009) 5603–5613;
(b) H. Wu, Y. Zhang, R. Yin, W. Zhao, X. Li, L. Qian, Magnetic negative permittivity with dielectric resonance in random Fe₃O₄@graphene-phenolic resin composites, Adv. Compos. Hybrid Mater. (2017) https://doi.org/10.1007/s42114-017-0014-1 in press, and;
(c) C. Cheng, R. Fan, Z. Wang, Q. Shao, X. Guo, P. Xie, Y. Yin, Y. Zhang, L. An, Y. Lei, J. Ryu, A. Shankar, Z. Guo, Tunable and weakly negative permittivity in carbon/silicon nitride composites with different carbonizing temperatures, Carbon 125 (2018) 103–112.

[15] K. Deshmukh, M.B. Ahamed, K.K. Sadasivuni, D. Ponnamma, M.A.-A. Al Maadeed, S.K. Khadheer Pasha, R.R. Deshmukh, K. Chidambaram, Graphene oxide reinforced poly (4-styrenesulfonic acid)/polyvinyl alcohol blend composites with enhanced dielectric properties for portable and flexible electronics, Mater. Chem. Phys. 186 (2017) 188–201.

[16] U. Khan, T.H. Kim, H. Ryu, W. Seung, S.W. Kim, Graphene tribotronics for electronic skin and touch screen applications, Adv. Mater. 29 (2017).

[17] S. Stankovich, D.A. Dikin, G.H.B. Dommett, K.M. Kohlhaas, E.J. Zimney, E.A. Stach, R.D. Piner, S.T. Nguyen, R.S. Ruoff, Graphene-based composite materials, Nature 442 (2006) 282–286.

[18] D. Li, M.B. Mueller, S. Gilje, R.B. Kaner, G.G. Wallace, Processable aqueous dispersions of graphene nanosheets, Nat. Nanotechnol. 3 (2008) 101–105.

[19] L. Wang, W.W. Wang, P. Fan, M.L. Zhou, J.T. Yang, F. Chen, M.Q. Zhong, Ionic liquid-modified graphene/poly(vinyl alcohol) composite with enhanced properties, J. Appl. Polym. Sci. 134 (2017).

[20] Y. Li, S. Wang, Q. Wang, Enhancement of tribological properties of polymer composites reinforced by functionalized graphene, Compos. Part B 120 (2017) 83–91.

[21] H. Bai, Y. Xu, L. Zhao, C. Li, G. Shi, Non-covalent functionalization of graphene sheets by sulfonated polyaniline, Chem. Commun. (2009) 1667–1669.

[22] J. Liang, Y. Huang, L. Zhang, Y. Wang, Y. Ma, T. Guo, Y. Chen, Molecular-level dispersion of graphene into poly(vinyl alcohol) and effective reinforcement of their nanocomposites, Adv. Funct. Mater. 19 (2009) 2297–2302.

[23] S. Stankovich, R.D. Piner, X. Chen, N. Wu, S.T. Nguyen, R.S. Ruoff, Stable aqueous dispersions of graphitic nanoplatelets via the reduction of exfoliated graphite oxide in the presence of poly(sodium 4-styrenesulfonate), J. Mater. Chem. 16 (2006) 155–158.

[24] S. Pei, H.-M. Cheng, The reduction of graphene oxide, Carbon 50 (2012) 3210–3228.

[25] X. Fan, W. Peng, Y. Li, X. Li, S. Wang, G. Zhang, F. Zhang, Deoxygenation of exfoliated graphite oxide under alkaline conditions: a green route to graphene preparation, Adv. Mater. 20 (2008) 4490–4493.

[26] M.J. Fernández-Merino, L. Guardia, J.I. Paredes, S. Villar-Rodil, P. Solís-Fernández, A. Martínez-Alonso, J.M.D. Tascón, Vitamin C is an ideal substitute for hydrazine in the reduction of graphene oxide suspensions, J. Phys. Chem. C 114 (2010) 6426–6432.

[27] W. Chen, L. Yan, P.R. Bangal, Chemical reduction of graphene oxide to graphene by sulfur-containing compounds, J. Phys. Chem. C 114 (2010) 19885–19890.

[28] S. Mallakpour, A. Abdolmaleki, S. Borandeh, Covalently functionalized graphene sheets with biocompatible natural amino acids, Appl. Surf. Sci. 307 (2014) 533–542.

[29] J.R. Lomeda, C.D. Doyle, D.V. Kosynkin, W.-F. Hwang, J.M. Tour, Diazonium functionalization of surfactant-wrapped chemically converted graphene sheets, J. Am. Chem. Soc. 130 (2008) 16201–16206.

[30] J. Guo, L. Ren, R. Wang, C. Zhang, Y. Yang, T. Liu, Water dispersible graphene noncovalently functionalized with tryptophan and its poly(vinyl alcohol) nanocomposite, Compos. Part B 42 (2011) 2130–2135.

[31] E. Jaworska, W. Lewandowski, J. Mieczkowski, K. Maksymiuk, A. Michalska, Non-covalently functionalized graphene for the potentiometric sensing of zinc ions, Analyst 137 (2012) 1895–1898.

[32] J.L. Vickery, A.J. Patil, S. Mann, Fabrication of graphene-polymer nanocomposites with higher-order three-dimensional architectures, Adv. Mater. 21 (2009) 2180–2184.

[33] S. Liu, Ou JF, Z.P. Li, S.R. Yang, J.Q. Wang, Layer-by-layer assembly and tribological property of multilayer ultrathin films constructed by modified graphene sheets and polyethyleneimine, Appl. Surf. Sci. 258 (2012) 2231–2236.

[34] W.S. Hummers, R.E. Offeman, Preparation of graphitic oxide, J. Am. Chem. Soc. 80 (1958) 1339.

[35] L.J. Cote, F. Kim, J. Huang, Langmuir-Blodgett assembly of graphite oxide single layers, J. Am. Chem. Soc. 131 (2009) 1043–1049.

[36] D.C. Marcano, D.V. Kosynkin, J.M. Berlin, A. Sinitskii, Z. Sun, A. Slesarev, L.B. Alemany, W. Lu, J.M. Tour, Improved synthesis of graphene oxide, ACS Nano 4 (2010) 4806–4814.

[37] J.-X. Zhang, Y.-X. Liang, X. Wang, H.-J. Zhou, S.-Y. Li, J. Zhang, Y. Feng, N. Lu, Q. Wang, Z. Guo, Strengthened epoxy resin with hyperbranched polyamine-ester anchored graphene oxide via novel phase transfer approach, Adv. Compos. Hybrid Mater. (2017) https://doi.org/10.1007/s42114-017-0007-0 in press.

[38] W.F. Zhao, J. Kong, H. Liu, Q. Zhuang, Gu JW, Z.H. Guo, Ultra-high thermally conductive and rapid heat responsive poly(benzobisoxazole) nanocomposites with self-aligned graphene, Nano 8 (2016) 19984–19993.

[39] D.S. Sutar, P.K. Narayanam, G. Singh, V.D. Botcha, S.S. Talwar, R.S. Srinivasa, S.S. Major, Spectroscopic studies of large sheets of graphene oxide and reduced graphene oxide monolayers prepared by Langmuir–Blodgett technique, Thin Solid Films 520 (2012) 5991–5996.

[40] S. Stankovich, D.A. Dikin, R.D. Piner, K.A. Kohlhaas, A. Kleinhammes, Y. Jia, Y. Wu, S.T. Nguyen, R.S. Ruoff, Synthesis of graphene-based nanosheets via chemical reduction of exfoliated graphite oxide, Carbon 45 (2007) 1558–1565.

[41] Z.X. Wang, X.B. Yang, Z.J. Cheng, Y.Y. Liu, L. Shao, L. Jiang, Simply realizing "water diode" Janus membranes for multifunctional smart applications, Mater. Horiz. 4 (2017) 701–708.

[42] C. Mao, J.R. Huang, Y.T. Zhu, W. Jiang, Q.X. Tang, X.J. Ma, Tailored parallel graphene stripes in plastic film with conductive anisotropy by shear-induced self-assembly, J. Phys. Chem. Lett. 4 (2013) 43–47.

[43] J.R. Huang, Y.T. Zhu, W. Jiang, Q.X. Tang, Parallel carbon nanotube stripes in polymer thin film with tunable microstructures and anisotropic conductive properties, Compos. Part A: Appl. Sci. Manuf. 69 (2015) 240–246.

[44] J. Guo, H. Song, H. Liu, C. Luo, Y. Ren, T. Ding, M.A. Khan, D.P. Young, X. Liu, X. Zhang, J. Kong, Z. Guo, Polypyrrole-interface-functionalized nano-magnetite epoxy nanocomposites as electromagnetic wave absorbers with enhanced flame retardancy, J. Mater. Chem. C 5 (2017) 5334–5344.

[45] A.C. Ferrari, J.C. Meyer, V. Scardaci, C. Casiraghi, M. Lazzeri, F. Mauri, S. Piscanec, D. Jiang, K.S. Novoselov, S. Roth, A.K. Geim, Raman spectrum of graphene and graphene layers, Phys. Rev. Lett. 97 (2006).

[46] X. An, T. Simmons, R. Shah, C. Wolfe, K.M. Lewis, M. Washington, S.K. Nayak, S. Talapatra, S. Kar, Stable aqueous dispersions of noncovalently functionalized graphene from graphite and their multifunctional high-performance applications, Nano Lett. 10 (2010) 4295–4301.

[47] L. Jiang, S. Islam, N.S. Korivi, Micro-patterning of nanocomposites of polymer and carbon nanotubes, Microelectron. Eng. 93 (2012) 10–14.

[48] I.Y. Prosanov, A.A. Matvienko, Study of PVA thermal destruction by means of IR and Raman spectroscopy, Phys. Solid State 52 (2010) 2203–2206.

[49] T. Zhou, F. Chen, C. Tang, H. Bai, Q. Zhang, H. Deng, Q. Fu, The preparation of high performance and conductive poly (vinyl alcohol)/graphene nanocomposite via reducing graphite oxide with sodium hydrosulfite, Compos. Sci. Technol. 71 (2011) 1266–1270.

[50] Y.-H. Yang, L. Bolling, M.A. Priolo, J.C. Grunlan, Super gas barrier and selectivity of graphene oxide-polymer multilayer thin films, Adv. Mater. 25 (2013) 503–508.

[51] H. Kim, A.A. Abdala, C.W. Macosko, Graphene/polymer nanocomposites, Macromolecules 43 (2010) 6515–6530.

[52] H.J. Salavagione, G. Martinez, M.A. Gomez, Synthesis of poly(vinyl alcohol)/reduced graphite oxide nanocomposites with improved thermal and electrical properties, J. Mater. Chem. 19 (2009) 5027–5032.

[53] J.-H. Yang, Y.-D. Lee, Highly electrically conductive rGO/PVA composites with a network dispersive nanostructure, J. Mater. Chem. 22 (2012) 8512–8517.

[54] J. Gu, W. Dong, Y. Tang, Y. Guo, L. Tang, J. Kong, S. Tadakamalla, B. Wang, Z. Guo, Ultralow dielectric, fluoride-containing cyanate ester resins with improved mechanical properties and high thermal and dimensional stabilities, J. Mater. Chem. C 5 (2017) 6929–6936.

[55] Gu JW, S. Xu, Q. Zhuang, Y.S. Tang, J. Kong, Hyperbranched polyborosilazane and boron nitride modified cyanate ester composite with low dielectric loss and desirable thermal conductivity, IEEE Trans. Dielectr. Electr. Insul. 24 (2017) 784–790.

[56] W. Wang, T. Sun, Y. Zhang, Y.-B. Wang, Substituent effects in the π···π interaction between graphene and benzene: an indication for the noncovalent functionalization of graphene, Comput. Theor. Chem. 1046 (2014) 64–69.

[57] C.A. Hunter, J.K.M. Sanders, The nature of .pi.-.pi. interactions, J. Am. Chem. Soc. 112 (1990) 5525–5534.

[58] J.W. Chen, X.H. Cui, Y.T. Zhu, W. Jiang, K.Y. Sui, Design of superior conductive polymer composite with precisely controlling carbon nanotubes at the interface of a co-continuous polymer blend via a balance of pi-pi interactions and dipole-dipole interactions, Carbon 114 (2017) 441–448.

[59] C. Mao, Y.T. Zhu, W. Jiang, Design of electrical conductive composites: tuning the morphology to improve the electrical properties of graphene filled immiscible polymer blends, ACS Appl. Mater. Interfaces 4 (2012) 5281–5286.